

## 1. TENSORIAL ASPECTS OF PHYSICAL PROPERTIES

The associated powers are calculated according to (1.7.3.8), which leads to

$$P(L) = m(n/2)(\varepsilon_o/\mu_o)^{1/2}|E_o|^2\pi w_o^2 \quad (1.7.3.38)$$

where  $m = 1$  for a flat distribution and  $m = 1/2$  for a Gaussian profile.

The nonlinear interaction is characterized by the conversion efficiency, which is defined as the ratio of the generated power to the power of one or several incident beams, according to the different kinds of interactions.

For pulsed beams, it is necessary to consider the temporal shape, usually Gaussian:

$$P(t) = P_c \exp(-2t^2/\tau^2) \quad (1.7.3.39)$$

where  $P_c$  is the peak power and  $\tau$  the half ( $1/e^2$ ) width.

For a repetition rate  $f$  ( $s^{-1}$ ), the average power  $\tilde{P}$  is then given by

$$\tilde{P} = P_c \tau f (\pi/2)^{1/2} = \tilde{E} f \quad (1.7.3.40)$$

where  $\tilde{E}$  is the energy per Gaussian pulse.

When the pulse shape is not well defined, it is suitable to consider the energies per pulse of the incident and generated waves for the definition of the conversion efficiency.

The interactions studied here are sum-frequency generation (SFG), including second harmonic generation (SHG:  $\omega + \omega = 2\omega$ ), cascading third harmonic generation (THG:  $\omega + 2\omega = 3\omega$ ) and direct third harmonic generation (THG:  $\omega + \omega + \omega = 3\omega$ ). The difference-frequency generation (DFG) is also considered, including optical parametric amplification (OPA) and oscillation (OPO).

We choose to analyse in detail the different parameters relative to conversion efficiency (figure of merit, acceptance bandwidths, walk-off effect *etc.*) for SHG, which is the prototypical second-order nonlinear interaction. This discussion will be valid for the other nonlinear processes of frequency generation which will be considered later.

### 1.7.3.3.2. Second harmonic generation (SHG)

According to Table 1.7.3.1, there are two types of phase matching for SHG: type I and type II (equivalent to type III).

The fundamental waves at  $\omega$  define the pump. Two situations are classically distinguished: the undepleted pump approximation, when the power conversion efficiency is sufficiently low to consider the fundamental power to be undepleted, and the depleted case for higher efficiency. There are different ways to realize SHG, as shown in Fig. 1.7.3.6: the simplest one is non-resonant SHG, outside the laser cavity; other ways are external or internal resonant cavity SHG, which allow an enhancement of the single-pass efficiency conversion.

#### 1.7.3.3.2.1. Non-resonant SHG with undepleted pump in the parallel-beam limit with a Gaussian transverse profile

We first consider the case where the crystal length is short enough to be located in the near-field region of the laser beam where the parallel-beam limit is a good approximation. We make another simplification by considering a propagation along a principal axis of the index surface: then the walk-off angle of each interacting wave is nil so that the three waves have the same coordinate system  $(X, Y, Z)$ .

The integration of equations (1.7.3.22) over the crystal length  $Z$  in the undepleted pump approximation, *i.e.*  $\partial E_1^\omega(X, Y, Z)/\partial Z = \partial E_2^\omega(X, Y, Z)/\partial Z = 0$ , with  $E_3^{2\omega}(X, Y, 0) = 0$ , leads to

$$|E_3^{2\omega}(X, Y, L)|^2 = \{K_3^{2\omega}[\varepsilon_o \chi_{\text{eff}}^{(2)}]\}^2 |E_1^\omega(X, Y, 0)E_2^\omega(X, Y, 0)|^2 \times L^2 \sin^2 c^2 [(\Delta k \cdot L)/2]. \quad (1.7.3.41)$$

(1.7.3.41) implies a Gaussian transversal profile for  $|E_3^{2\omega}(X, Y, L)|$  if  $|E_1^\omega(X, Y, 0)|$  and  $|E_2^\omega(X, Y, 0)|$  are Gaussian. The three beam radii are related by  $(1/w_{o3}^2) = (1/w_{o1}^2) + (1/w_{o2}^2)$ , so if we assume that the two fundamental beams have the same radius  $w_o^\omega$ , which is not an approximation for type I, then  $w_o^{2\omega} = [w_o^\omega/(2^{1/2})]$ . Two incident beams with a flat distribution of radius  $w_o^\omega$  lead to the generation of a flat harmonic beam with the same radius  $w_o^{2\omega} = w_o^\omega$ .

The integration of (1.7.3.41) according to (1.7.3.36)–(1.7.3.38) for a Gaussian profile gives in the SI system

$$P^{2\omega}(L) = BP_1^\omega(0)P_2^\omega(0)\frac{L^2}{w_o^2}\sin^2 c^2\left(\frac{\Delta k \cdot L}{2}\right) \\ B = \frac{32\pi}{\varepsilon_o c} \frac{2N-1}{N} \frac{d_{\text{eff}}^2}{\lambda_\omega^2} \frac{T_3^{2\omega} T_1 T_2}{n_3^{2\omega} n_1^\omega n_2^\omega}, \quad (W^{-1}) \quad (1.7.3.42)$$

where  $c = 3 \times 10^8 \text{ m s}^{-1}$ ,  $\varepsilon_o = 8.854 \times 10^{-12} \text{ A s V}^{-1} \text{ m}^{-1}$  and so  $(32\pi/\varepsilon_o c) = 37.85 \times 10^3 \text{ V A}^{-1}$ .  $L$  (m) is the crystal length in the direction of propagation.  $\Delta k = k_3^{2\omega} - k_1^\omega - k_2^\omega$  is the phase mismatch.  $n_3^{2\omega}$ ,  $n_1^\omega$  and  $n_2^\omega$  are the refractive indices at the harmonic and fundamental wavelengths  $\lambda_{2\omega}$  and  $\lambda_\omega$  ( $\mu\text{m}$ ): for the phase-matching case,  $\Delta k = 0$ ,  $n_3^{2\omega} = n^-(2\omega)$ ,  $n_1^\omega = n_2^\omega = n^+(\omega)$  for type I (the two incident fundamental beams have the same polarization contained in  $\Pi^+$ , with the harmonic polarization contained in  $\Pi^-$ ) and  $n_1^\omega = n^+(\omega) \neq n_2^\omega = n^-(\omega)$  for type II (the two solicited eigen modes at the fundamental wavelength are in  $\Pi^+$  and  $\Pi^-$ , with the harmonic polarization contained in  $\Pi^-$ ).  $T_3^{2\omega}$ ,  $T_1$  and  $T_2$  are the transmission coefficients given by  $T_i = 4n_i/(n_i + 1)^2$ .  $d_{\text{eff}}$  ( $\text{pm V}^{-1}$ ) =  $(1/2)\chi_{\text{eff}} = (1/2)[F^{(2)} \cdot \chi^{(2)}]$  is the effective coefficient given by (1.7.3.30) and (1.7.3.31).  $P_1^\omega(0)$  and  $P_2^\omega(0)$  are the two incident fundamental powers, which are not necessarily equal for type II; for type I we have obviously  $P_1^\omega(0) = P_2^\omega(0) = (P_{\text{tot}}^\omega/2)$ .  $N$  is the number of independently oscillating modes at the fundamental wavelength: every longitudinal mode at the harmonic pulsation can be generated by many combinations of two fundamental modes; the  $(2N-1)/N$  factor takes into account the fluctuations between these longitudinal modes (Bloembergen, 1963).

The powers in (1.7.3.42) are instantaneous powers  $P(t)$ .

The second harmonic (SH) conversion efficiency,  $\eta_{\text{SHG}}$ , is usually defined as the ratio of peak powers  $P^{2\omega}(L)/P_{\text{c,tot}}^\omega(0)$ , or as the ratio of the pulse total energy  $\tilde{E}^{2\omega}(L)/\tilde{E}_{\text{tot}}^\omega(0)$ . For Gaussian temporal profiles, the SH ( $1/e^2$ ) pulse duration  $\tau_{2\omega}$  is equal to  $\tau_\omega/(2^{1/2})$ , because  $P_{2\omega}$  is proportional to  $P_\omega^2$ , and so, according to (1.7.3.40), the pulse average energy conversion efficiency is  $1/(2^{1/2})$  smaller than the peak power conversion efficiency given by (1.7.3.42). Note that the pulse total energy conversion efficiency is equivalent to the average power conversion efficiency  $\tilde{P}^{2\omega}(L)/\tilde{P}_{\text{tot}}^\omega(0)$ , with  $\tilde{P} = \tilde{E} \cdot f$  where  $f$  is the repetition rate.

Formula (1.7.3.42) shows the importance of the contribution of the linear optical properties to the nonlinear process. Indeed, the field tensor  $F^{(2)}$ , the transmission coefficients  $T_i$  and the phase mismatch  $\Delta k$  only depend on the refractive indices in the direction of propagation considered.

(i) *Figure of merit.*

The contribution of  $F^{(2)}$  was discussed previously, where it was shown that the field tensor is nil in particular directions of propagation or everywhere for particular crystal classes and configurations of polarization (even if the nonlinearity  $\chi^{(2)}$  is high).

The field tensor  $F^{(2)}$  of SHG can be written with the contracted notation of  $d^{(2)}$ ; according to Table 1.7.3.1 and to the contraction

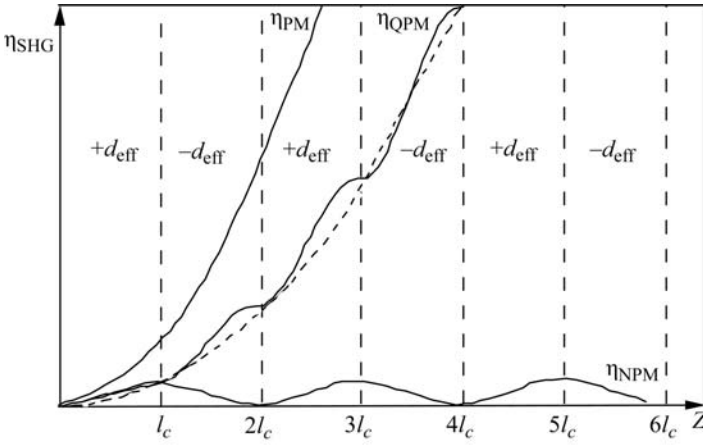


Fig. 1.7.3.7. Spatial growth evolution of second harmonic conversion efficiency,  $\eta_{\text{SHG}}$ , for non phase matching (NPM),  $\Delta k \neq 0$ , and phase matching (PM),  $\Delta k = 0$ , in a 'continuous' crystal, and for quasi phase matching (QPM) in a periodic structure. The dashed curve corresponds to  $(4/\pi^2)\eta_{\text{PM}}(Z)$  where  $\eta_{\text{PM}}$  is the conversion efficiency of the phase-matched SHG.  $l_c = \pi/\Delta k$  is the coherence length.

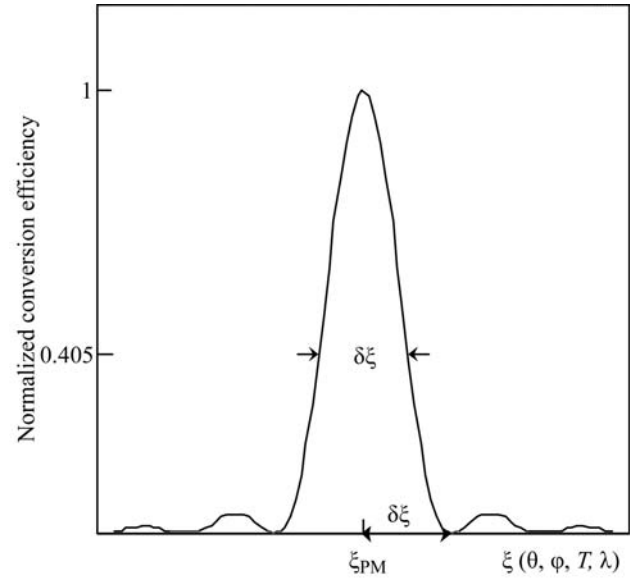


Fig. 1.7.3.8. Conversion efficiency evolution as a function of  $\xi$  for a given crystal length.  $\xi$  denotes the angle ( $\theta$  or  $\varphi$ ), the temperature ( $T$ ) or the wavelength ( $\lambda$ ).  $\xi_{\text{PM}}$  represents the parameter allowing phase matching.

conventions given in Section 1.7.2.2, the contracted field-tensor components for the phase-matched SHG are

$$\begin{aligned} F_{i1} &= \mathbf{e}_i^-(2\omega)[\mathbf{e}_x^+(\omega)]^2 \\ F_{i2} &= \mathbf{e}_i^-(2\omega)[\mathbf{e}_y^+(\omega)]^2 \\ F_{i3} &= \mathbf{e}_i^-(2\omega)[\mathbf{e}_z^+(\omega)]^2 \\ F_{i4} &= 2\mathbf{e}_i^-(2\omega)\mathbf{e}_y^+(\omega)\mathbf{e}_z^+(\omega) \\ F_{i5} &= 2\mathbf{e}_i^-(2\omega)\mathbf{e}_x^+(\omega)\mathbf{e}_z^+(\omega) \\ F_{i6} &= 2\mathbf{e}_i^-(2\omega)\mathbf{e}_x^+(\omega)\mathbf{e}_y^+(\omega) \end{aligned}$$

for type I and

$$\begin{aligned} F_{i1} &= \mathbf{e}_i^-(2\omega)\mathbf{e}_x^+(\omega)\mathbf{e}_x^-(\omega) \\ F_{i2} &= \mathbf{e}_i^-(2\omega)\mathbf{e}_y^+(\omega)\mathbf{e}_y^-(\omega) \\ F_{i3} &= \mathbf{e}_i^-(2\omega)\mathbf{e}_z^+(\omega)\mathbf{e}_z^-(\omega) \\ F_{i4} &= \mathbf{e}_i^-(2\omega)[\mathbf{e}_y^+(\omega)\mathbf{e}_z^-(\omega) + \mathbf{e}_y^-(\omega)\mathbf{e}_z^+(\omega)] \\ F_{i5} &= \mathbf{e}_i^-(2\omega)[\mathbf{e}_x^+(\omega)\mathbf{e}_z^-(\omega) + \mathbf{e}_x^-(\omega)\mathbf{e}_z^+(\omega)] \\ F_{i6} &= \mathbf{e}_i^-(2\omega)[\mathbf{e}_x^+(\omega)\mathbf{e}_y^-(\omega) + \mathbf{e}_x^-(\omega)\mathbf{e}_y^+(\omega)] \end{aligned}$$

for type II, with  $i = (1, 2, 3)$  for  $F_{ij}$ , corresponding to  $i = (x, y, z)$  for  $\mathbf{e}_i^-(2\omega)$ .

The ratio  $d_{\text{eff}}^2/n_3^2\omega n_1^2\omega n_2^2\omega$  in formula (1.7.3.42) is called the figure of merit of the direction considered. The effective coefficient is given in Section 1.7.5 for the main nonlinear crystals and for chosen SHG wavelengths.

(ii) *Effect of the phase mismatch.*

The interference function  $\sin^2(\Delta kL/2)$  is a maximum and equal to unity only for  $\Delta k = 0$ , which defines the phase-matching condition. Fig. 1.7.3.7 shows the effect of the phase mismatch on the growth of second harmonic conversion efficiency,  $\eta_{\text{SHG}}$ , with interaction distance  $Z$ .

The conversion efficiency has a  $Z^2$  dependence in the case of phase matching. The harmonic power oscillates around  $Z^2$  for quasi phase matching, but is reduced by a factor of  $4/\pi^2$  compared with that of phase-matched interaction (Fejer *et al.*, 1992).

An SHG phase-matching direction ( $\theta_{\text{PM}}, \varphi_{\text{PM}}$ ) for given fundamental wavelength ( $\lambda_{\text{PM}}$ ) and type of interaction, I or II, is defined at a given temperature ( $T_{\text{PM}}$ ). It is important to consider the effect of deviation of  $\Delta k$  from 0 due to variations of angles ( $\theta_{\text{PM}} \pm d\theta, \varphi_{\text{PM}} \pm d\varphi$ ), of temperature ( $T_{\text{PM}} \pm dT$ ) and of wave-

length ( $\lambda_{\text{PM}} \pm d\lambda$ ) on the conversion efficiency. The quantities that characterize these effects are the acceptance bandwidths  $\delta\xi$  ( $\xi = \theta, \varphi, T, \lambda$ ), usually defined as the deviation from the phase-matching value  $\xi_{\text{PM}}$  leading to a phase-mismatch variation  $\Delta k$  from 0 to  $2\pi/L$ , where  $L$  is the crystal length. Then  $\delta\xi$  is also the full width of the peak efficiency curve plotted as a function of  $\xi$  at 0.405 of the maximum, as shown in Fig. 1.7.3.8.

Thus  $L\delta\xi$  is a characteristic of the phase-matching direction. Small angular, thermal and spectral dispersion of the refractive indices lead to high acceptance bandwidths. The higher  $L\delta\xi$ , the lower is the decrease of the conversion efficiency corresponding to a given angular shift, to the heating of the crystal due to absorption or external heating, or to the spectral bandwidth of the fundamental beam.

The knowledge of the angular, thermal and spectral dispersion of the refractive indices allows an estimation of  $\delta\xi$  by expanding  $\Delta k$  in a Taylor series about  $\xi_{\text{PM}}$ :

$$\frac{2\pi}{L} = \Delta k = \left. \frac{\partial(\Delta k)}{\partial\xi} \right|_{\xi_{\text{PM}}} \delta\xi + \frac{1}{2} \left. \frac{\partial^2(\Delta k)}{\partial\xi^2} \right|_{\xi_{\text{PM}}} (\delta\xi)^2 + \dots \quad (1.7.3.43)$$

When the second- and higher-order differential terms in (1.7.3.43) are negligible, the phase matching is called critical (CPM), because  $L\delta\xi \simeq |2\pi/[\partial(\Delta k)/\partial\xi]_{\xi_{\text{PM}}}|$  is small. For the particular cases where  $\partial(\Delta k)/\partial\xi|_{\xi_{\text{PM}}} = 0$ ,  $L\delta\xi = \{|4\pi L/[\partial^2(\Delta k)/\partial\xi^2]_{\xi_{\text{PM}}}| \}^{1/2}$  is larger than the CPM acceptance and the phase matching is called non-critical (NCPM) for the parameter  $\xi$  considered.

We first consider the case of angular acceptances. In uniaxial crystals, the refractive indices do not vary in  $\varphi$ , leading to an infinite  $\varphi$  angular acceptance bandwidth.  $\delta\theta$  is then the only one to consider. For directions of propagation out of the principal plane ( $\theta_{\text{PM}} \neq \pi/2$ ), the phase matching is critical. According to the expressions of  $n_o$  and  $n_e(\theta)$  given in Section 1.7.3.1, we have

$$(1) \text{ for type I in positive crystals, } n_e(\theta, \omega) = n_o(2\omega) \text{ and}$$

$$L\delta\theta \simeq 2\pi/[-(\omega/c)n_o^3(2\omega)[n_e^{-2}(\omega) - n_o^{-2}(\omega)] \sin 2\theta_{\text{PM}}]; \quad (1.7.3.44)$$

(2) for type II in positive crystals,  $2n_o(2\omega) = n_e(\theta, \omega) + n_o(\omega)$  and

## 1. TENSORIAL ASPECTS OF PHYSICAL PROPERTIES

$$L\delta\theta \simeq 2\pi/\{-(\omega/2c)[2n_o(2\omega) - n_o(\omega)]^3 \times [n_e^{-2}(\omega) - n_o^{-2}(\omega)] \sin 2\theta_{\text{PM}}\}; \quad (1.7.3.45)$$

(3) for type I in negative crystals,  $n_e(\theta, 2\omega) = n_o(\omega)$  and

$$L\delta\theta \simeq 2\pi/\{-(\omega/c)n_o^3(\omega)[n_e^{-2}(2\omega) - n_o^{-2}(2\omega)] \sin 2\theta_{\text{PM}}\}; \quad (1.7.3.46)$$

(4) for type II in negative crystals,  $2n_e(\theta, 2\omega) = n_e(\theta, \omega) + n_o(\omega)$  and

$$L\delta\theta \simeq |2\pi/\{-(\omega/c)n_e^3(\theta, 2\omega)[n_e^{-2}(2\omega) - n_o^{-2}(2\omega)] \sin 2\theta_{\text{PM}} + (\omega/2c)n_e^3(\theta, \omega)[n_e^{-2}(\omega) - n_o^{-2}(\omega)] \sin 2\theta_{\text{PM}}\}|. \quad (1.7.3.47)$$

CPM acceptance bandwidths are small, typically about one mrad cm, as shown in Section 1.7.5 for the classical nonlinear crystals.

When  $\theta_{\text{PM}} = \pi/2$ ,  $\partial\Delta k/\partial\theta = 0$  and the phase matching is non-critical:

(1) for type I in positive crystals,  $n_e(\omega) = n_o(2\omega)$  and

$$L\delta\theta \simeq (2\pi L/\{-(\omega/c)n_o^3(2\omega)[n_e^{-2}(\omega) - n_o^{-2}(\omega)]\})^{1/2}; \quad (1.7.3.48)$$

(2) for type II in positive crystals,  $2n_o(2\omega) = n_e(\omega) + n_o(\omega)$  and

$$L\delta\theta \simeq (2\pi L/\{-(\omega/2c)n_e^3(\omega)[n_e^{-2}(\omega) - n_o^{-2}(\omega)]\})^{1/2}; \quad (1.7.3.49)$$

(3) for type I in negative crystals,  $n_o(\omega) = n_e(2\omega)$  and

$$L\delta\theta \simeq (2\pi L/\{(\omega/c)n_o^3(\omega)[n_e^{-2}(2\omega) - n_o^{-2}(2\omega)]\})^{1/2}; \quad (1.7.3.50)$$

(4) for type II in negative crystals,  $2n_e(2\omega) = n_e(\omega) + n_o(\omega)$  and

$$L\delta\theta \simeq (|2\pi L/\{-(\omega/c)n_e^3(2\omega)[n_e^{-2}(2\omega) - n_o^{-2}(2\omega)] + (\omega/2c)n_e^3(\omega)[n_e^{-2}(\omega) - n_o^{-2}(\omega)]\}|)^{1/2}. \quad (1.7.3.51)$$

Values of NCPM acceptance bandwidths are given in Section 1.7.5 for the usual crystals. From the previous expressions for CPM and NCPM angular acceptances, it appears that the angular bandwidth is all the smaller since the birefringence is high.

The situation is obviously more complex in the case of biaxial crystals. The  $\varphi$  acceptance bandwidth is not infinite, leading to a smaller anisotropy of the angular acceptance in comparison with uniaxial crystals. The expressions of the  $\theta$  and  $\varphi$  acceptance bandwidths have the same form as for the uniaxial class only in the principal planes. The phase matching is critical (CPM) for all directions of propagation out of the principal axes  $x$ ,  $y$  and  $z$ : in this case, the mismatch  $\Delta k$  is a linear function of small angular deviations from the phase-matching direction as for uniaxial crystals. There exist six possibilities of NCPM for SHG, types I and II along the three principal axes, corresponding to twelve different index conditions (Hobden, 1967):

(1) for positive biaxial crystals

$$\begin{array}{ll} \text{Type I (x)} & n_{2\omega}^y = n_\omega^z \\ \text{Type I (y)} & n_{2\omega}^x = n_\omega^z \\ \text{Type I (z)} & n_{2\omega}^x = n_\omega^y \\ \text{Type II (x)} & n_{2\omega}^y = \frac{1}{2}(n_\omega^y + n_\omega^z) \\ \text{Type II (y)} & n_{2\omega}^x = \frac{1}{2}(n_\omega^x + n_\omega^z) \\ \text{Type II (z)} & n_{2\omega}^x = \frac{1}{2}(n_\omega^x + n_\omega^y); \end{array} \quad (1.7.3.52)$$

(2) for negative biaxial crystals

$$\begin{array}{ll} \text{Type I (x)} & n_{2\omega}^z = n_\omega^y \\ \text{Type I (y)} & n_{2\omega}^z = n_\omega^x \\ \text{Type I (z)} & n_{2\omega}^y = n_\omega^x \\ \text{Type II (x)} & n_{2\omega}^z = \frac{1}{2}(n_\omega^y + n_\omega^z) \\ \text{Type II (y)} & n_{2\omega}^z = \frac{1}{2}(n_\omega^x + n_\omega^z) \\ \text{Type II (z)} & n_{2\omega}^y = \frac{1}{2}(n_\omega^x + n_\omega^y). \end{array}$$

The NCPM angular acceptances along the three principal axes of biaxial crystals can be deduced from the expressions relative to the uniaxial class by the following substitutions:

Along the  $x$  axis:

$$L\delta\varphi \text{ (type I } > 0) = (1.7.3.50) \text{ with } n_o(\omega) \rightarrow n_x(\omega),$$

$$n_e(2\omega) \rightarrow n_y(2\omega) \text{ and } n_o(2\omega) \rightarrow n_x(2\omega)$$

$$L\delta\theta \text{ (type I } > 0) = (1.7.3.48) \text{ with } n_o(2\omega) \rightarrow n_y(2\omega),$$

$$n_e(\omega) \rightarrow n_z(\omega) \text{ and } n_o(\omega) \rightarrow n_x(\omega)$$

$$L\delta\varphi \text{ (type II } > 0) = (1.7.3.51) \text{ with } n_e \rightarrow n_y \text{ and } n_o \rightarrow n_x$$

$$L\delta\theta \text{ (type II } > 0) = (1.7.3.49) \text{ with } n_e(\omega) \rightarrow n_z(\omega)$$

$$\text{and } n_o(\omega) \rightarrow n_x(\omega)$$

$$L\delta\varphi \text{ (type I } < 0) = (1.7.3.48) \text{ with } n_o(2\omega) \rightarrow n_z(2\omega),$$

$$n_e(\omega) \rightarrow n_x(\omega) \text{ and } n_o(\omega) \rightarrow n_y(\omega)$$

$$L\delta\theta \text{ (type I } < 0) = (1.7.3.50) \text{ with } n_o(\omega) \rightarrow n_y(\omega),$$

$$n_e(2\omega) \rightarrow n_z(2\omega) \text{ and } n_o(2\omega) \rightarrow n_x(2\omega)$$

$$L\delta\varphi \text{ (type II } < 0) = (1.7.3.49) \text{ with } n_e(\omega) \rightarrow n_x(\omega)$$

$$\text{and } n_o(\omega) \rightarrow n_y(\omega)$$

$$L\delta\theta \text{ (type II } < 0) = (1.7.3.51) \text{ with } n_e \rightarrow n_z \text{ and } n_o \rightarrow n_x.$$

Along the  $y$  axis:

$L\delta\varphi$  is the same as along the  $x$  axis for all interactions

$$L\delta\theta \text{ (type I } > 0) = (1.7.3.48) \text{ with } n_o(2\omega) \rightarrow n_x(2\omega),$$

$$n_e(\omega) \rightarrow n_z(\omega) \text{ and } n_o(\omega) \rightarrow n_y(\omega)$$

$$L\delta\theta \text{ (type II } > 0) = (1.7.3.49) \text{ with } n_e(\omega) \rightarrow n_z(\omega)$$

$$\text{and } n_o(\omega) \rightarrow n_y(\omega)$$

$$L\delta\theta \text{ (type I } < 0) = (1.7.3.50) \text{ with } n_o(\omega) \rightarrow n_x(\omega),$$

$$n_e(2\omega) \rightarrow n_z(2\omega) \text{ and } n_o(2\omega) \rightarrow n_y(2\omega)$$

$$L\delta\theta \text{ (type II } < 0) = (1.7.3.51) \text{ with } n_e \rightarrow n_z \text{ and } n_o \rightarrow n_y.$$

Along the  $z$  axis:

$$L\delta\theta_{xz} \text{ (type I } > 0) = (1.7.3.48) \text{ with } n_o(2\omega) \rightarrow n_y(2\omega),$$

$$n_e(\omega) \rightarrow n_x(\omega) \text{ and } n_o(\omega) \rightarrow n_z(\omega)$$

$$L\delta\theta_{yz} \text{ (type I } > 0) = (1.7.3.48) \text{ with } n_o(2\omega) \rightarrow n_x(2\omega),$$

$$n_e(\omega) \rightarrow n_y(\omega) \text{ and } n_o(\omega) \rightarrow n_z(\omega)$$

$$L\delta\theta_{xz} \text{ (type II } > 0) = (1.7.3.49) \text{ with } n_e(\omega) \rightarrow n_x(\omega)$$

$$\text{and } n_o(\omega) \rightarrow n_z(\omega)$$

$$L\delta\theta_{yz} \text{ (type II } > 0) = (1.7.3.49) \text{ with } n_e(\omega) \rightarrow n_y(\omega)$$

$$\text{and } n_o(\omega) \rightarrow n_z(\omega)$$

$$L\delta\theta_{xz} \text{ (type I } < 0) = (1.7.3.50) \text{ with } n_o(\omega) \rightarrow n_y(\omega),$$

$$n_e(2\omega) \rightarrow n_z(2\omega) \text{ and } n_o(2\omega) \rightarrow n_x(2\omega)$$

$$L\delta\theta_{yz} \text{ (type I } < 0) = (1.7.3.50) \text{ with } n_o(\omega) \rightarrow n_x(\omega),$$

$$n_e(2\omega) \rightarrow n_z(2\omega) \text{ and } n_o(2\omega) \rightarrow n_y(2\omega)$$

## 1.7. NONLINEAR OPTICAL PROPERTIES

$L\delta\theta_{xz}$  (type II < 0) = (1.7.3.51) with  $n_e \rightarrow n_x$  and  $n_o \rightarrow n_z$

$L\delta\theta_{yz}$  (type II < 0) = (1.7.3.51) with  $n_e \rightarrow n_y$  and  $n_o \rightarrow n_z$ .

The above formulae are relative to the internal angular acceptance bandwidths. The external acceptance angles are enlarged by a factor of approximately  $n(\omega)$  for type I or  $[n_1(\omega) + n_2(\omega)]/2$  for type II, due to refraction at the input plane face of the crystal. The angular acceptance is an important issue connected with the accuracy of cutting of the crystal.

Temperature tuning is a possible alternative for achieving NCPM in a few materials. The corresponding temperatures for different interactions are given in Section 1.7.5.

Another alternative is to use a special non-collinear configuration known as one-beam non-critical non-collinear phase matching (OBNC): it is non-critical with respect to the phase-matching angle of one of the input beams (referred to as the non-critical beam). It has been demonstrated that the angular acceptance bandwidth for the non-critical beam is exceptionally large, for example about 50 times that for the critical beam for type-I SHG at 1.338  $\mu\text{m}$  in 3-methyl-4-nitropyridine-*N*-oxide (POM) (Dou *et al.*, 1992).

The typical values of thermal acceptance bandwidth, given in Section 1.7.5, are of the order of 0.5 to 50 K cm. The thermal acceptance is an important issue for the stability of the harmonic power when the absorption at the wavelengths concerned is high or when temperature tuning is used for the achievement of angular NCPM. Typical spectral acceptance bandwidths for SHG are given in Section 1.7.5. The values are of the order of 1 nm cm, which is much larger than the linewidth of a single-frequency laser, except for some diode or for sub-picosecond lasers with a large spectral bandwidth.

Note that a degeneracy of the first-order temperature or spectral derivatives ( $\partial\Delta k/\partial T|_{T_{PM}} = 0$  or  $\partial\Delta k/\partial\lambda|_{\lambda_{PM}} = 0$ ) can occur and lead to thermal or spectral NCPM.

Consideration of the phase-matching function  $\lambda_{PM} = f(\xi_{PM})$ , where  $\chi_{PM} = T_{PM}, \theta_{PM}, \varphi_{PM}$  or all other dispersion parameters of the refractive indices, is useful for a direct comparison of the situation of non-criticality of the phase matching relative to  $\lambda_{PM}$  and to the other parameters  $\xi_{PM}$ : a nil derivative of  $\lambda_{PM}$  with respect to  $\xi_{PM}$ , *i.e.*  $d\lambda_{PM}/d\xi_{PM} = 0$  at the point  $(\lambda_{PM}^0, \xi_{PM}^0)$ , means that the phase matching is non-critical with respect to  $\xi_{PM}$  and so strongly critical with respect to  $\lambda_{PM}$ , *i.e.*  $d\xi_{PM}/d\lambda_{PM} = \infty$  at this point. Then, for example, an angular NCPM direction is a spectral CPM direction and the reverse is also so.

(iii) *Effect of spatial walk-off.*

The interest of the NCPM directions is increased by the fact that the walk-off angle of any wave is nil: the beam overlap is complete inside the nonlinear crystal. Under CPM, the interacting waves propagate with different walk-off angles: the conversion efficiency is then attenuated because the different Poynting vectors are not collinear and the beams do not overlap. Type I and type II are not equivalent in terms of walk-off angles. For type I, the two fundamental waves have the same polarization  $\mathbf{E}^+$  and the same walk-off angle  $\rho^+$ , which is different from the harmonic one; thus the coordinate systems that are involved in equations (1.7.3.22) are  $(X_1, Y_1, Z) = (X_2, Y_2, Z) = (X_\omega^+, Y_\omega^+, Z)$  and  $(X_3, Y_3, Z) = (X_{2\omega}^-, Y_{2\omega}^-, Z)$ . For type II, the two fundamental waves have necessarily different walk-off angles  $\rho^+$  and  $\rho^-$ , which forbids the nonlinear interaction beyond the plane where the two fundamental beams are completely separated. In this case we have three different coordinate systems:  $(X_1, Y_1, Z) = (X_\omega^+, Y_\omega^+, Z)$ ,  $(X_2, Y_2, Z) = (X_\omega^-, Y_\omega^-, Z)$  and  $(X_3, Y_3, Z) = (X_{2\omega}^-, Y_{2\omega}^-, Z)$ .

The three coordinate systems are linked by the refraction angles  $\rho$  of the three waves as explained in Section 1.7.3.2.1. We consider Gaussian transverse profiles: the electric field amplitude is then given by (1.7.3.37). In these conditions, the integration of (1.7.3.22) over  $(X, Y, Z)$  by assuming  $\tan \rho = \rho$ , the non-deple-

tion of the pump and, in the case of phase matching,  $\Delta k = 0$  leads to the efficiency  $\eta_{\text{SHG}}(L)$  given by formula (1.7.3.42) with  $\sin^2(\Delta kL/2) = 1$  and multiplied by the factor  $[G(L, w_o, \rho)]/[\cos^2 \rho(2\omega)]$  where  $\rho(2\omega)$  is the harmonic walk-off angle and  $G(L, w_o, \rho)$  is the walk-off attenuation function.

For type I, the walk-off attenuation is given by (Boyd *et al.*, 1965)

$$G_I(t) = (\pi^{1/2}/t) \operatorname{erf}(t) - (1/t^2)[1 - \exp(-t^2)]$$

with

$$t = (\rho L/w_o) \quad (1.7.3.53)$$

and

$$\operatorname{erf}(x) = (2/\pi^{1/2}) \int_0^x \exp(-t^2) dt.$$

For uniaxial crystals,  $\rho = \rho^e(2\omega)$  for a *2oe* interaction and  $\rho = \rho^o(\omega)$  for a *2eo* interaction. For the biaxial class,  $\rho = \rho^e(2\omega)$  for a *2oe* interaction and  $\rho = \rho^o(\omega)$  for a *2eo* interaction in the *xz* and *yz* planes,  $\rho = \rho^o(\omega)$  for a *2oe* interaction and  $\rho = \rho^o(2\omega)$  for a *2eo* interaction in the *xy* plane. For any direction of propagation not contained in the principal planes of a biaxial crystal, the fundamental and harmonic waves have nonzero walk-off angles, respectively  $\rho^+(\omega)$  and  $\rho^-(2\omega)$ . In this case, (1.7.3.53) can be used with  $\rho = |\rho^+(\omega) - \rho^-(2\omega)|$ .

(a) For small  $t$  ( $t \ll 1$ ),  $G_I(t) \simeq 1$  and  $P^{2\omega}(L) \equiv L^2$ ,

(b) For large  $t$  ( $t \gg 1$ ),  $G_I(t) \simeq (\pi^{1/2}/t)$  and so  $P^{2\omega}(L) \equiv L/\rho$  according to (1.7.3.42) with  $\Delta k = 0$ .

For type II, we have (Mehendale & Gupta, 1988)

$$G_{II}(t) = (2/\pi^{1/2}) \int_{-\infty}^{+\infty} F^2(a, t) da$$

with

$$F(a, t) = (1/t) \exp(-a^2) \int_0^t \exp[-(a + \tau)^2] d\tau \quad (1.7.3.54)$$

and

$$a = \frac{r}{w_o} \quad \tau = \frac{\rho u}{w_o} \quad t = \frac{\rho L}{w_o}.$$

$r$  and  $u$  are the Cartesian coordinates in the walk-off plane where  $u$  is collinear with the three wavevectors, *i.e.* the phase-matching direction.

$\rho = \rho^e(\omega)$  for (*oeo*) in uniaxial crystals and in the *xz* and *yz* planes of biaxial crystals.  $\rho = \rho^o(\omega)$  in the *xy* plane of biaxial crystals for an (*eo*e) interaction.

For the interactions where  $\rho^-(2\omega)$  and  $\rho^-(\omega)$  are nonzero, we assume that they are close and contained in the same plane, which is generally the case. Then we classically take  $\rho$  to be the maximum value between  $|\rho^-(2\omega) - \rho^+(\omega)|$  and  $|\rho^-(\omega) - \rho^+(\omega)|$ . This approximation concerns the (*eo*e) configuration of polarization in uniaxial crystals and for biaxial crystals in the *xz* and *yz* planes, in the *xy* plane for (*oeo*) and out of the principal planes for all the configurations of polarization.

The exact calculation of  $G$ , which takes into account the three walk-off angles,  $\rho^-(\omega)$ ,  $\rho^+(\omega)$  and  $\rho^-(2\omega)$ , was performed in the case where these three angles were coplanar (Asaumi, 1992). The exact calculation in the case of  $\text{KTiOPO}_4$  (KTP) for type-II SHG at 1.064  $\mu\text{m}$  gives the same result for  $L/z_R < 1$  as for one angle defined as previously (Fève *et al.*, 1995), which includes the parallel-beam limit  $L/z_R < 0.3-0.4$ :  $z_R = [k(\omega)w_o^2]/2$  is the Rayleigh length of the fundamental beam inside the crystal.

(a) For  $t \ll 1$ ,  $G_{II}(t) \simeq 1$ , leading to the  $L^2$  dependence of  $P^{2\omega}(L)$ .

# 1. TENSORIAL ASPECTS OF PHYSICAL PROPERTIES

(b) For  $t \gg 1$ ,  $G_{II}(t) \simeq (t_a^2/t^2)$  with  $t_a = [(2)^{1/2} \arctan(2^{1/2})]^{1/2}$ , corresponding to a saturation of  $P^{2\omega}(L)$  because of the walk-off between the two fundamental beams as shown in Fig. 1.7.3.9.

The saturation length,  $L_{sat}$ , is defined as  $2.3t_a w_o/\rho$ , which corresponds to the length beyond which the SHG conversion

efficiency varies less than 1% from its saturation value  $BP^{\omega}(0)t_a^2/\rho^2$ .

The complete splitting of the two fundamental beams does not occur for type I, making it more suitable than type II for strong focusing. The fundamental beam splitting for type II also leads to a saturation of the acceptance bandwidths  $\delta\xi$  ( $\xi = \theta, \varphi, T, \lambda$ ), which is not the case for type I (Fève *et al.*, 1995). The walk-off angles also modify the transversal distribution of the generated harmonic beam (Boyd *et al.*, 1965; Mehendale & Gupta, 1988): the profile is larger than that of the fundamental beam for type I, contrary to type II.

The walk-off can be compensated by the use of two crystals placed one behind the other, with the same length and cut in the same CPM direction (Akhmanov *et al.*, 1975): the arrangement of the second crystal is obtained from that of the first one by a  $\pi$  rotation around the direction of propagation or around the direction orthogonal to the direction of propagation and contained in the walk-off plane as shown in Fig. 1.7.3.10 for the particular case of type II (*oeo*) in a positive uniaxial crystal out of the  $xy$  plane.

The twin-crystal device is potentially valid for both types I and II. The relative sign of the effective coefficients of the twin

crystals depends on the configuration of polarization, on the relative arrangement of the two crystals and on the crystal class. The interference between the waves generated in the two crystals is destructive and so cancels the SHG conversion efficiency if the two effective coefficients have opposite signs: it is always the case for certain crystal classes and configurations of polarization (Moore & Koch, 1996).

Such a tandem crystal was used, for example, with  $\text{KTiOPO}_4$  (KTP) for type-II SHG at  $\lambda_\omega = 1.3 \mu\text{m}$  ( $\rho = 2.47^\circ$ ) and  $\lambda_{2\omega} = 2.532 \mu\text{m}$  ( $\rho = 2.51^\circ$ ): the conversion efficiency was about 3.3 times the efficiency in a single crystal of length  $2L$ , where  $L$  is the length of each crystal of the twin device (Zondy *et al.*, 1994). The two crystals have to be antireflection coated or contacted in order to avoid Fresnel reflection losses.

Non-collinear phase matching is another method allowing a reduction of the walk-off, but only in the case of type II (Dou *et al.*, 1992). Fig. 1.7.3.11 illustrates the particular case of (*oeo*) type-II SHG for a propagation out of the  $xy$  plane of a uniaxial crystal, or in the  $xz$  or  $yz$  plane of a biaxial crystal.

In the configuration of special non-collinear phase matching, the angle between the fundamental beams inside the crystal is chosen to be equal to the walk-off angle  $\rho$ . Then the associated Poynting vectors  $\mathbf{S}^{\omega,o}$  and  $\mathbf{S}^{\omega,e}$  are along the same direction, while that of the generated wave deviates from them only by approximately  $\rho/2$ . The calculation performed in the case of special non-collinear phase matching indicates that it is possible to increase type-II SHG conversion efficiency by 17% for near-field undepleted Gaussian beams (Dou *et al.*, 1992). Another advantage of such geometry is to turn type II into a pseudo type I with respect to the walk-off,

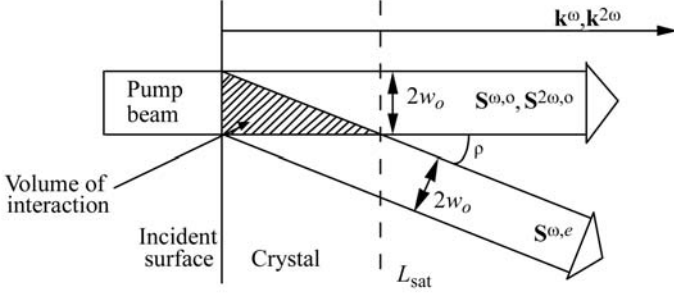


Fig. 1.7.3.9. Beam separation in the particular case of type-II (*oeo*) SHG out of the  $xy$  plane of a positive uniaxial crystal or in the  $xz$  and  $yz$  planes of a positive biaxial crystal.  $\mathbf{S}^{\omega,o}$ ,  $\mathbf{S}^{\omega,e}$  and  $\mathbf{S}^{2\omega,o}$  are the fundamental and harmonic Poynting vectors;  $\mathbf{k}^\omega$  and  $\mathbf{k}^{2\omega}$  are the associated wavevectors collinear to the CPM direction.  $w_o$  is the fundamental beam radius and  $\rho$  is the walk-off angle.  $L_{sat}$  is the saturation length.

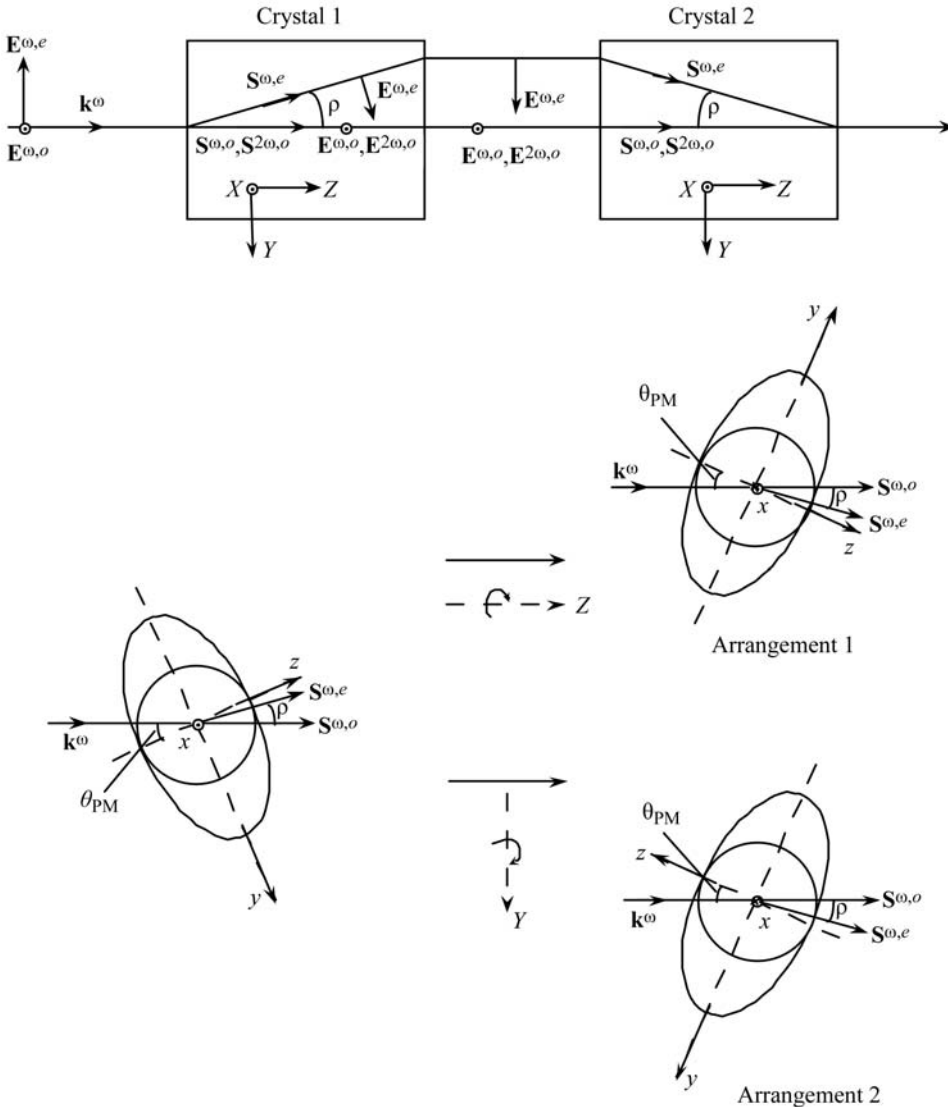


Fig. 1.7.3.10. Twin-crystal device allowing walk-off compensation for a direction of propagation  $\theta_{PM}$  in the  $yz$  plane of a positive uniaxial crystal.  $(X, Y, Z)$  is the wave frame and  $(x, y, z)$  is the optical frame. The index surface is given in the  $yz$  plane.  $\mathbf{k}^\omega$  is the incident fundamental wavevector. The refracted wavevectors  $\mathbf{k}^{\omega,o}$ ,  $\mathbf{k}^{\omega,e}$  and  $\mathbf{k}^{2\omega,o}$  are collinear and along  $\mathbf{k}^\omega$ .  $\mathbf{S}^{\omega,o}$ ,  $\mathbf{S}^{\omega,e}$  and  $\mathbf{S}^{2\omega,o}$  are the Poynting vectors of the fundamental and harmonic waves.  $\mathbf{E}^{\omega,o}$ ,  $\mathbf{E}^{\omega,e}$  and  $\mathbf{E}^{2\omega,o}$  are the electric field vectors.  $\rho$  is the walk-off angle.

## 1.7. NONLINEAR OPTICAL PROPERTIES

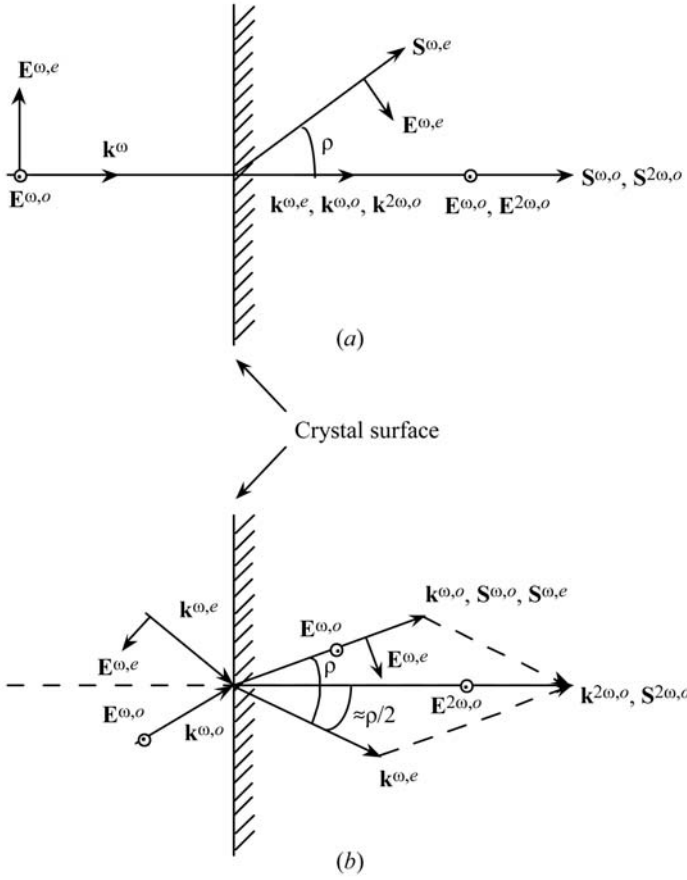


Fig. 1.7.3.11. Comparison between (a) collinear and (b) special non-collinear phase matching for (o eo) type-II SHG.  $\mathbf{k}^{\omega,o}$ ,  $\mathbf{k}^{\omega,e}$  and  $\mathbf{k}^{2\omega,o}$  are the wavevectors,  $\mathbf{S}^{\omega,o}$ ,  $\mathbf{S}^{\omega,e}$  and  $\mathbf{S}^{2\omega,o}$  are the Poynting vectors of the fundamental and harmonic waves, and  $\mathbf{E}^{\omega,o}$ ,  $\mathbf{E}^{\omega,e}$  and  $\mathbf{E}^{2\omega,o}$  are the electric field vectors;  $\rho$  is the walk-off angle in the collinear case and the angle between  $\mathbf{k}^{\omega,o}$  and  $\mathbf{k}^{\omega,e}$  inside the crystal for the non-collinear interaction.

because the saturation phenomenon of type-II CPM is avoided.

(iv) *Effect of temporal walk-off.*

Even if the SHG is phase matched, the fundamental and harmonic group velocities,  $v_g(\omega) = \partial\omega/\partial k$ , are generally mismatched. This has no effect with continuous wave (c.w.) lasers. For pulsed beams, the temporal separation of the different beams during the propagation can lead to a decrease of the temporal overlap of the pulses. Indeed, this walk-off in the time domain affects the conversion efficiency when the pulse separations are close to the pulse durations. Then after a certain distance,  $L_\tau$ , the pulses are completely separated, which entails a saturation of the conversion efficiency, for both types I and II (Tomov *et al.*, 1982). Three group velocities must be considered for type II. Type I is simpler, because the two fundamental waves have the same velocity, so  $L_\tau = \tau/[v_g^{-1}(\omega) - v_g^{-1}(2\omega)]$ , which defines the optimum crystal length, where  $\tau$  is the pulse duration. For type-I SHG of 532 nm in  $\text{KH}_2\text{PO}_4$  (KDP),  $v_g(266 \text{ nm}) = 1.84 \times 10^8 \text{ m s}^{-1}$  and  $v_g(532 \text{ nm}) = 1.94 \times 10^8 \text{ m s}^{-1}$ , so  $L_\tau = 3.5 \text{ mm}$  for 1 ps. For the usual nonlinear crystals, the temporal walk-off must be taken into account for pico- and femtosecond pulses.

### 1.7.3.3.2.2. Non-resonant SHG with undepleted pump and transverse and longitudinal Gaussian beams

We now consider the general situation where the crystal length can be larger than the Rayleigh length.

The Gaussian electric field amplitudes of the two eigen electric field vectors inside the nonlinear crystal are given by

$$E^\pm(X, Y, Z) = E_o^\pm \frac{w_o}{w(Z)} \exp \left[ -\frac{(X + \rho^+ Z)^2 + (Y + \rho^- Z)^2}{w^2(Z)} \right] \times \exp \left( i \left\{ k^\pm Z - \arctan(Z/z_R) + \frac{k^\pm [(X + \rho^+ Z)^2 + (Y + \rho^- Z)^2]}{2Z[1 + (z_R^2/Z^2)]} \right\} \right) \quad (1.7.3.55)$$

with  $\rho^- = 0$  for  $E^+$  and  $\rho^+ = 0$  for  $E^-$ .

$(X, Y, Z)$  is the wave frame defined in Fig. 1.7.3.1.  $E_o^\pm$  is the scalar complex amplitude at  $(X, Y, Z) = (0, 0, 0)$  in the vibration planes  $\Pi^\pm$ .

We consider the refracted waves  $E^+$  and  $E^-$  to have the same longitudinal profile inside the crystal. Then the  $(1/e^2)$  beam radius is given by  $w(Z) = w_o[1 + (Z^2/z_R^2)]$ , where  $w_o$  is the minimum beam radius located at  $Z = 0$  and  $z_R = kw_o^2/2$ , with  $k = (k^+ + k^-)/2$ ;  $z_R$  is the Rayleigh length, the length over which the beam radius remains essentially collimated;  $k^\pm$  are the wavevectors at the wavelength  $\lambda$  in the direction of propagation  $Z$ . The far-field half divergence angle is  $\Delta\alpha = 2/kw_o$ .

The coordinate systems of (1.7.3.22) are identical to those of the parallel-beam limit defined in (iii).

In these conditions and by assuming the undepleted pump approximation, the integration of (1.7.3.22) over  $(X, Y, Z)$  leads to the following expression of the power conversion efficiency (Zondy, 1991):

$$\eta_{\text{SHG}}(L) = \frac{P^{2\omega}(L)}{P^\omega(0)} = CLP^\omega(0) \frac{h(L, w_o, \rho, f, \Delta k)}{\cos^2 \rho_{2\omega}}$$

with

$$C = 5.95 \times 10^{-2} \frac{2N - 1}{N} \frac{d_{\text{eff}}^2}{\lambda_\omega^3} \frac{n_1^\omega + n_2^\omega}{2} \frac{T_3^{2\omega} T_1^\omega T_2^\omega}{n_3^{2\omega} n_1^\omega n_2^\omega} \quad (\text{W}^{-1} \text{ m}^{-1}) \quad (1.7.3.56)$$

in the same units as equation (1.7.3.42).

For type I,  $n_1^\omega = n_2^\omega$ ,  $T_1^\omega = T_2^\omega$ , and for type II  $n_1^\omega \neq n_2^\omega$ ,  $T_1^\omega \neq T_2^\omega$ .

The attenuation coefficient is written

$$h(L, w_o, \rho, f, \Delta k) = [2z_R(\pi)^{1/2}/L] \int_{-\infty}^{+\infty} |H(a)|^2 \exp(-4a^2) da$$

with

$$H(a) = \frac{1}{(2\pi)^{1/2}} \int_{-fL/z_R}^{L(1-f)/z_R} \frac{d\tau}{1 + i\tau} \exp \left[ -\gamma^2 \left( \tau + \frac{fL}{z_R} \right)^2 - i\sigma\tau \right]$$

$$\text{for type I: } \gamma = 0 \text{ and } \sigma = \Delta k z_R + 4 \frac{\rho z_R}{w_o} a$$

$$\text{for type II: } \gamma = \frac{\rho z_R}{w_o(2)^{1/2}} \text{ and } \sigma = \Delta k z_R + 2 \frac{\rho z_R}{w_o} a,$$

$$(1.7.3.57)$$

where  $f$  gives the position of the beam waist inside the crystal:  $f = 0$  at the entrance and  $f = 1$  at the exit surface. The definition and approximations relative to  $\rho$  are the same as those discussed for the parallel-beam limit.  $\Delta k$  is the mismatch parameter, which takes into account first a possible shift of the pump beam direction from the collinear phase-matching direction and secondly the distribution of mismatch, including collinear and non-collinear interactions, due to the divergence of the beam, even if the beam axis is phase-matched.

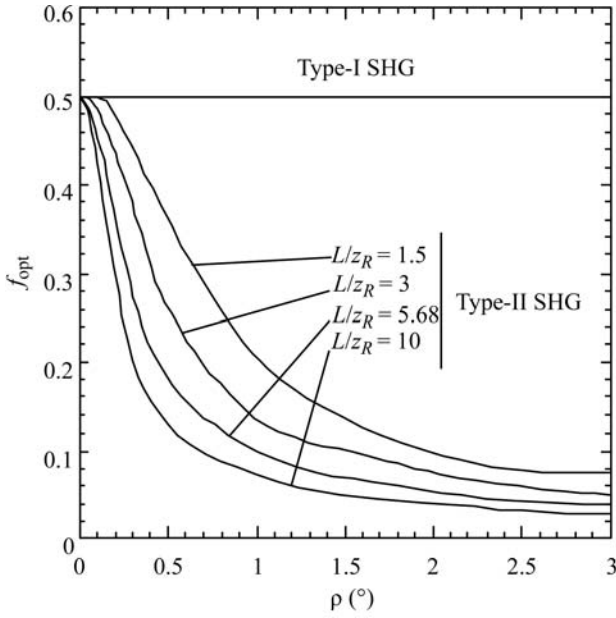


Fig. 1.7.3.12. Position  $f_{\text{opt}}$  of the beam waist for different values of walk-off angles and  $L/z_R$ , leading to an optimum SHG conversion efficiency. The value  $f_{\text{opt}} = 0.5$  corresponds to the middle of the crystal and  $f_{\text{opt}} = 0$  corresponds to the entrance surface (Fève & Zondy, 1996).

The computation of  $h(L, w_o, \rho, f, \Delta k)$  allows an optimization of the SHG conversion efficiency which takes into account  $L/z_R$ , the waist location  $f$  inside the crystal and the phase mismatch  $\Delta k$ .

Fig. 1.7.3.12 shows the calculated waist location which allows an optimal SHG conversion efficiency for types I and II with optimum phase matching. From Fig. 1.7.3.12, it appears that the optimum waist location for type I, which leads to an optimum conversion efficiency, is exactly at the centre of the crystal,  $f_{\text{opt}} = 0.5$ . For type II, the focusing ( $L/z_R$ ) is stronger and the walk-off angle is larger, and the optimum waist location is nearer the entrance of the crystal. These facts can be physically understood: for type I, there is no walk-off for the fundamental beam, so the whole crystal length is efficient and the symmetrical configuration is obviously the best one; for type II, the two fundamental rays can be completely separated in the waist area, which has the strongest intensity, when the waist location is far from the entrance face; for a waist location nearer the entrance, the waist area can be selected and the enlargement of the beams from this area allows a spatial overlap up to the exit face, which leads to a higher conversion efficiency.

The divergence of the pump beam imposes non-collinear interactions such that it could be necessary to shift the direction of propagation of the beam from the collinear phase-matching direction in order to optimize the conversion efficiency. This leads to the definition of an optimum phase-mismatch parameter  $\Delta k_{\text{opt}} (\neq 0)$  for a given  $L/z_R$  and a fixed position of the beam waist  $f$  inside the crystal.

The function  $h(L, w_o, \rho, f_{\text{opt}}, \Delta k_{\text{opt}})$ , written  $h_m(B, L)$ , is plotted in Fig. 1.7.3.13 as a function of  $L/z_R$  for different values of the walk-off parameter, defined as  $B = (1/2)\rho\{(k_o^\omega + k_e^\omega)/2\}L^{1/2}$ , at the optimal waist location and phase mismatch.

Consider first the case of angular NCPM ( $B = 0$ ) where type-I and -II conversion efficiencies obviously have the same  $L/z_R$  evolutions. An optimum focusing at  $L/z_R = 5.68$  exists which defines the optimum focusing  $z_{R_{\text{opt}}}$  for a given crystal length or the optimal length  $L_{\text{opt}}$  for a given focusing. The conversion efficiency decreases for  $L/z_R > 5.68$  because the increase of the ‘average’ beam radius over the crystal length due to the strong focusing becomes more significant than the increased peak power in the waist area.

In the case of angular CPM ( $B \neq 0$ ), the  $L/z_R$  variation of type-I conversion efficiency is different from that of type II. For

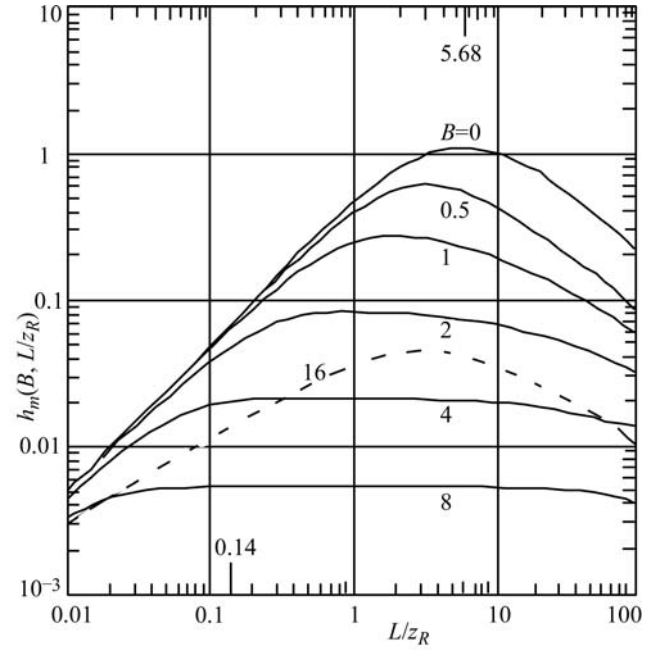


Fig. 1.7.3.13. Optimum walk-off function  $h_m(B, L)$  as a function of  $L/z_R$  for various values of  $B = (1/2)\rho\{(k_o^\omega + k_e^\omega)/2\}L^{1/2}$ . The curve at  $B = 0$  is the same for both type-I and type-II phase matching. The full lines at  $B \neq 0$  are for type II and the dashed line at  $B = 16$  is for type I. (From Zondy, 1990).

type I, as  $B$  increases, the efficiency curves keep the same shape, with their maxima abscissa shifting from  $L/z_R = 5.68$  ( $B = 0$ ) to  $2.98$  ( $B = 16$ ) as the corresponding amplitudes decrease. For type II, an optimum focusing becomes less and less apparent, while  $(L/z_R)_{\text{opt}}$  shifts to much smaller values than for type I for the same variation of  $B$ ; the decrease of the maximum amplitude is stronger in the case of type II. The calculation of the conversion efficiency as a function of the crystal length  $L$  at a fixed  $z_R$  shows a saturation for type II, in contrast to type I. The saturation occurs at  $B \simeq 3$  with a corresponding focusing parameter  $L/z_R \simeq 0.4$ , which is the limit of validity of the parallel-beam approximation. These results show that weak focusing is suitable for type II, whereas type I allows higher focusing.

The curves of Fig. 1.7.3.14 give a clear illustration of the walk-off effect in several usual situations of crystal length, walk-off angle and Gaussian laser beam. The SHG conversion efficiency is calculated from formula (1.7.3.56) and from the function (1.7.3.57) at  $f_{\text{opt}}$  and  $\Delta k_{\text{opt}}$ .

#### 1.7.3.3.2.3. Non-resonant SHG with depleted pump in the parallel-beam limit

The analytical integration of the three coupled equations (1.7.3.22) with depletion of the pump and phase mismatch has only been done in the parallel-beam limit and by neglecting the walk-off effect (Armstrong *et al.*, 1962; Eckardt & Reintjes, 1984; Eimerl, 1987; Milton, 1992). In this case, the three coordinate systems of equations (1.7.3.22) are identical,  $(X, Y, Z)$ , and the general solution may be written in terms of the Jacobian elliptic function  $\text{sn}(m, \alpha)$ .

For the simple case of type I, *i.e.*  $E_1^\omega(X, Y, Z) = E_2^\omega(X, Y, Z) = E^\omega(X, Y, Z) = E_{\text{tot}}^\omega(X, Y, Z)/(2^{1/2})$ , the exit second harmonic intensity generated over a length  $L$  is given by (Eckardt & Reintjes, 1984)

$$I^{2\omega}(X, Y, L) = I_{\text{tot}}^\omega(X, Y, 0) T^{2\omega} T^\omega v_b^2 \text{sn}^2 \left[ \frac{\Gamma(X, Y)L}{v_b}, v_b^4 \right]. \quad (1.7.3.58)$$

## 1.7. NONLINEAR OPTICAL PROPERTIES

$I_{\text{tot}}^\omega(X, Y, 0) = 2I^\omega(X, Y, 0)$  is the total initial fundamental intensity,  $T^{2\omega}$  and  $T^\omega$  are the transmission coefficients,

$$\frac{1}{v_b} = \frac{\Delta s}{4} + \left[ 1 + \left( \frac{\Delta s}{4} \right)^2 \right]^{1/2}$$

with

$$\Delta s = (k^{2\omega} - k^\omega)/\Gamma$$

and

$$\Gamma(X, Y) = \frac{\omega d_{\text{eff}}}{cn^{2\omega}} (T^\omega)^{1/2} |E_{\text{tot}}^\omega(X, Y, 0)|. \quad (1.7.3.59)$$

For the case of phase matching ( $k^\omega = k^{2\omega}$ ,  $T^\omega = T^{2\omega}$ ), we have  $\Delta s = 0$  and  $v_b = 1$ , and the Jacobian elliptic function  $\text{sn}(m, 1)$  is equal to  $\tanh(m)$ . Then formula (1.7.3.58) becomes

$$I^{2\omega}(X, Y, L) = I_{\text{tot}}^\omega(X, Y, 0) (T^\omega)^2 \tanh^2[\Gamma(X, Y)L], \quad (1.7.3.60)$$

where  $\Gamma(X, Y)$  is given by (1.7.3.59).

The exit fundamental intensity  $I^\omega(X, Y, L)$  can be established easily from the harmonic intensity (1.7.3.60) according to the Manley–Rowe relations (1.7.2.40), *i.e.*

$$I^\omega(X, Y, L) = I_{\text{tot}}^\omega(X, Y, 0) (T^\omega)^2 \text{sech}^2[\Gamma(X, Y)L]. \quad (1.7.3.61)$$

For small  $\Gamma L$ , the functions  $\tanh^2(\Gamma L) \simeq \Gamma^2 L^2$  and  $\text{sn}^2[(\Gamma L/v_b), v_b^4] \simeq \sin^2(\Gamma L/v_b)$  with  $v_b \simeq 2/\Delta s$ .

The first consequence of formulae (1.7.3.58)–(1.7.3.59) is that the various acceptance bandwidths decrease with increasing  $\Gamma L$ . This fact is important in relation to all the acceptances but in particular for the thermal and angular ones. Indeed, high efficiencies are often reached with high power, which can lead to an important heating due to absorption. Furthermore, the divergence of the beams, even small, creates a significant dephasing: in this case, and even for a propagation along a phase-matching direction, formula (1.7.3.60) is not valid and may be replaced by (1.7.3.58) where  $k(2\omega) - k(\omega)$  is considered as the ‘average’ mismatch of a parallel beam.

In fact, there always exists a residual mismatch due to the divergence of real beams, even if not focused, which forbids asymptotically reaching a 100% conversion efficiency:  $I^{2\omega}(L)$  increases as a function of  $\Gamma L$  until a maximum value has been reached and then decreases;  $I^{2\omega}(L)$  will continue to rise and fall as  $\Gamma L$  is increased because of the periodic nature of the Jacobian elliptic sine function. Thus the maximum of the conversion efficiency is reached for a particular value  $(\Gamma L)_{\text{opt}}$ . The determination of  $(\Gamma L)_{\text{opt}}$  by numerical computation allows us to define the optimum incident fundamental intensity  $I_{\text{opt}}^\omega$  for a given phase-matching direction, characterized by  $K$ , and a given crystal length  $L$ .

The crystal length must be optimized in order to work with an incident intensity  $I_{\text{opt}}^\omega$  smaller than the damage threshold intensity  $I_{\text{dam}}^\omega$  of the nonlinear crystal, given in Section 1.7.5 for the main materials.

Formula (1.7.3.57) is established for type I. For type II, the second harmonic intensity is also an  $\text{sn}^2$  function where the

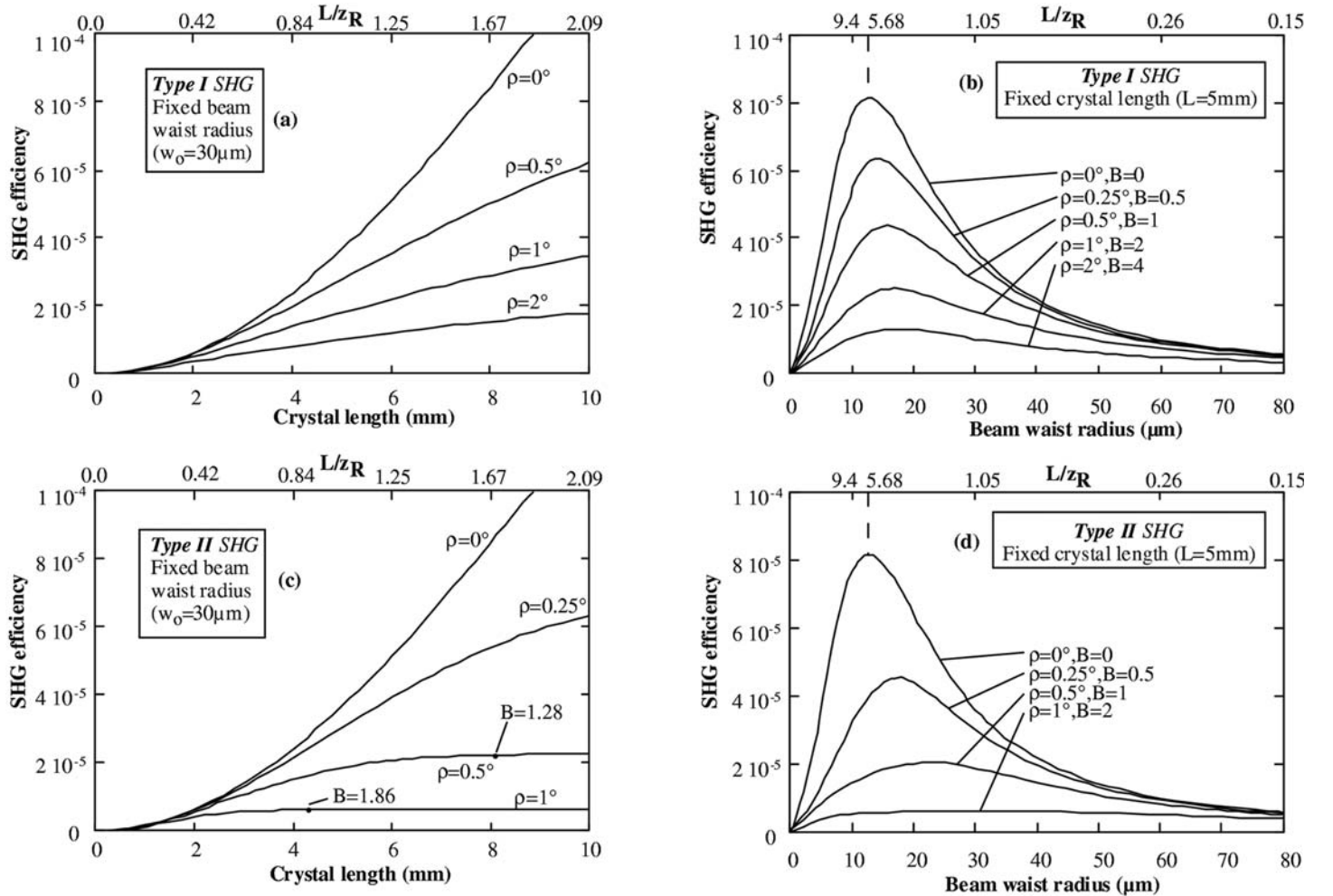


Fig. 1.7.3.14. Type-I and -II conversion efficiencies calculated as a function of  $L/z_R$  for different typical walk-off angles  $\rho$ : (a) and (c) correspond to a fixed focusing condition ( $w_0 = 30 \mu\text{m}$ ); the curves (b) and (d) are plotted for a constant crystal length ( $L = 5 \text{ mm}$ ); all the calculations are performed with the same effective coefficient ( $d_{\text{eff}} = 1 \text{ pm V}^{-1}$ ), refractive indices ( $n_3^2 n_1^\omega n_2^\omega = 5.83$ ) and fundamental power [ $P_\omega(0) = 1 \text{ W}$ ].  $B$  is the walk-off parameter defined in the text (Fève & Zondy, 1996).

## 1. TENSORIAL ASPECTS OF PHYSICAL PROPERTIES

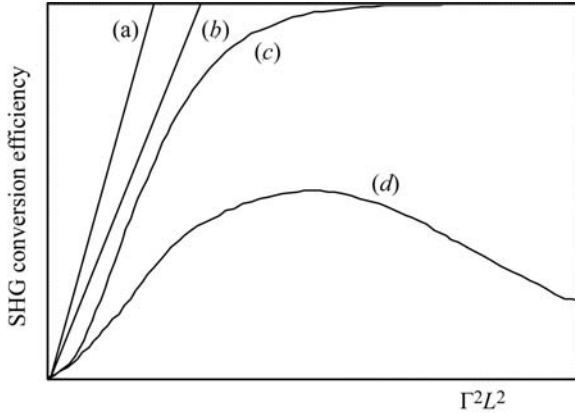


Fig. 1.7.3.15. Schematic SHG conversion efficiency for different situations of pump depletion and dephasing. (a) No depletion, no dephasing,  $\eta = \Gamma^2 L^2$ ; (b) no depletion with constant dephasing  $\delta$ ,  $\eta = \Gamma^2 L^2 \sin^2 c^2 \delta$ ; (c) depletion without dephasing,  $\eta = \tanh^2(\Gamma L)$ ; (d) depletion and dephasing,  $\eta = \eta_m \text{sn}^2(\Gamma L/v_b, v_b^4)$ .

intensities of the two fundamental beams  $I_1^\omega(X, Y, 0)$  and  $I_2^\omega(X, Y, 0)$ , which are not necessarily equal, are taken into account (Eimerl, 1987): the  $\tanh^2$  function is valid only if perfect phase matching is achieved and if  $I_1^\omega(X, Y, 0) = I_2^\omega(X, Y, 0)$ , these conditions being never satisfied in real cases.

The situations described above are summarized in Fig. 1.7.3.15.

We give the example of type-II SHG experiments performed with a 10 Hz injection-seeded single-longitudinal-mode ( $N = 1$ ) 1064 nm Nd:YAG (Spectra-Physics DCR-2A-10) laser equipped with super Gaussian mirrors; the pulse is 10 ns in duration and is near a Gaussian single-transverse mode, the beam radius is 4 mm, non-focused and polarized at  $\pi/4$  to the principal axes of a 10 mm long KTP crystal ( $L\delta\theta = 15$  mrad cm,  $L\delta\varphi = 100$  mrad cm). The fundamental energy increases from 78 mJ ( $62$  MW cm $^{-2}$ ) to 590 mJ ( $470$  MW cm $^{-2}$ ), which corresponds to the damage of the exit surface of the crystal; for each experiment, the crystal was rotated in order to obtain the maximum conversion efficiency. The peak power SHG conversion efficiency is estimated from the measured energy conversion efficiency multiplied by the ratio between the fundamental and harmonic pulse duration ( $\tau_\omega/\tau_{2\omega} = 2^{1/2}$ ). It increases from 50% at  $63$  MW cm $^{-2}$  to a maximum value of 85% at  $200$  MW cm $^{-2}$  and decreases for higher intensities, reaching 50% at  $470$  MW cm $^{-2}$  (Boulanger, Fejer *et al.*, 1994).

The integration of the intensity profiles (1.7.3.58) and (1.7.3.60) is obvious in the case of incident fundamental beams with a flat energy distribution (1.7.3.36). In this case, the fundamental and harmonic beams inside the crystal have the same profile and radius as the incident beam. Thus the powers are obtained from formulae (1.7.3.58) and (1.7.3.60) by expressing the intensity and electric field modulus as a function of the power, which is given by (1.7.3.38) with  $m = 1$ .

For a Gaussian incident fundamental beam, (1.7.3.37), the fundamental and harmonic beams are not Gaussian (Eckardt & Reintjes, 1984; Pliszka & Banerjee, 1993).

All the previous intensities are the peak values in the case of pulsed beams. The relation between average and peak powers, and then SHG efficiencies, is much more complicated than the ratio  $\tau^{2\omega}/\tau^\omega$  of the undepleted case.

### 1.7.3.3.2.4. Resonant SHG

When the single-pass conversion efficiency SHG is too low, with c.w. lasers for example, it is possible to put the nonlinear crystal in a Fabry-Perot cavity external to the pump laser or directly inside the pump laser cavity, as shown in Figs. 1.7.3.6(b) and (c). The second solution, described later, is generally used because the available internal pump intensity is much larger.

We first recall some basic and simplified results of laser cavity theory without a nonlinear medium. We consider a laser in which one mirror is 100% reflecting and the second has a transmission  $T$  at the laser pulsation  $\omega$ . The power within the cavity,  $P_{\text{in}}(\omega)$ , is evaluated at the steady state by setting the round-trip saturated gain of the laser equal to the sum of all the losses. The output laser cavity,  $P_{\text{out}}(\omega)$ , is given by (Siegman, 1986)

$$P_{\text{out}}(\omega) = TP_{\text{in}}(\omega)$$

with

$$P_{\text{in}}(\omega) = \frac{2g_o L' - (\gamma + T)}{2S(T + \gamma)}. \quad (1.7.3.62)$$

$L'$  is the laser medium length,  $g_o = \sigma N_o$  is the small-signal gain coefficient per unit length of laser medium,  $\sigma$  is the stimulated-emission cross section,  $N_o$  is the population inversion without oscillation,  $S$  is a saturation parameter characteristic of the nonlinearity of the laser transition, and  $\gamma = \gamma_L = 2\alpha_L L' + \beta$  is the loss coefficient where  $\alpha_L$  is the laser material absorption coefficient per unit length and  $\beta$  is another loss coefficient including absorption in the mirrors and scattering in both the laser medium and mirrors. For given  $g_o$ ,  $S$ ,  $\alpha_L$ ,  $\beta$  and  $L'$ , the output power reaches a maximum value for an optimal transmission coefficient  $T_{\text{opt}}$  defined by  $[\partial P_{\text{out}}(\omega)/\partial T]_{T_{\text{opt}}} = 0$ , which gives

$$T_{\text{opt}} = (2g_o L' \gamma)^{1/2} - \gamma. \quad (1.7.3.63)$$

The maximum output power is then given by

$$P_{\text{out}}^{\text{max}}(\omega) = (1/2S)[(2g_o L')^{1/2} - \gamma^{1/2}]^2. \quad (1.7.3.64)$$

In an intracavity SHG device, the two cavity mirrors are 100% reflecting at  $\omega$  but one mirror is perfectly transmitting at  $2\omega$ . The presence of the nonlinear medium inside the cavity then leads to losses at  $\omega$  equal to the round-trip-generated second harmonic (SH) power: half of the SH produced flows in the forward direction and half in the backward direction. Hence the highly transmitting mirror at  $2\omega$  is equivalent to a nonlinear transmission coefficient at  $\omega$  which is equal to twice the single-pass SHG conversion efficiency  $\eta_{\text{SHG}}$ .

The fundamental power inside the cavity  $P_{\text{in}}(\omega)$  is given at the steady state by setting, for a round trip, the saturated gain equal to the sum of the linear and nonlinear losses.  $P_{\text{in}}(\omega)$  is then given by (1.7.3.62), where  $T$  and  $\gamma$  are (Geusic *et al.*, 1968; Smith, 1970)

$$T = 2\eta_{\text{SHG}} = [P_{\text{out}}(2\omega)/P_{\text{in}}(\omega)] \quad (1.7.3.65)$$

and

$$\gamma = \gamma_L + \gamma_{NL}. \quad (1.7.3.66)$$

$\eta_{\text{SHG}}$  is the single-pass conversion efficiency.  $\gamma_L$  and  $\gamma_{NL}$  are the loss coefficients at  $\omega$  of the laser medium and of the nonlinear crystal, respectively.  $L$  is the nonlinear medium length. The two faces of the nonlinear crystal are assumed to be antireflection-coated at  $\omega$ .

In the undepleted pump approximation, the backward and forward power generated outside the nonlinear crystal at  $2\omega$  is

$$P_{\text{out}}(2\omega) = 2KP_{\text{in}}^2(\omega) \quad (1.7.3.67)$$

with

$$K = B(L^2/w_o^2) \sin^2(\Delta k L/2),$$

where

$$B = \frac{32\pi 2N - 1}{\epsilon_o c} \frac{d_{\text{eff}}^2}{N} \frac{T_3^{2\omega} T_1^\omega T_2^\omega}{\lambda_\omega^2 n_3^{2\omega} n_1^\omega n_2^\omega} \quad (\text{W}^{-1}).$$

## 1.7. NONLINEAR OPTICAL PROPERTIES

The intracavity SHG conversion efficiency is usually defined as the ratio of the SH output power to the maximum output power that would be obtained from the laser without the nonlinear crystal by optimal linear output coupling.

Maximizing (1.7.3.67) with respect to  $K$  according to (1.7.3.62), (1.7.3.65) and (1.7.3.66) gives (Perkins & Fahlen, 1987)

$$K_{\text{opt}} = (\gamma_L + \gamma_{NL})S \quad (1.7.3.68)$$

and

$$P_{\text{out}}^{\text{max}}(2\omega) = (1/2S)[(2g_o L')^{1/2} - (\gamma_L + \gamma_{NL})^{1/2}]^2. \quad (1.7.3.69)$$

(1.7.3.69) shows that for the case where  $\gamma_{NL} \ll \gamma_L$  ( $\gamma \simeq \gamma_L$ ), the maximum SH power is identically equal to the maximum fundamental power, (1.7.3.64), available from the same laser for the same value of loss, which, according to the previous definition of the intracavity efficiency, corresponds to an SHG conversion efficiency of 100%.  $P_{\text{out}}^{\text{max}}(2\omega)$  strongly decreases as the losses ( $\gamma_L + \gamma_{NL}$ ) increase. Thus an efficient intracavity device requires the reduction of all losses at  $\omega$  and  $2\omega$  to an absolute minimum.

(1.7.3.68) indicates that  $K_{\text{opt}}$  is independent of the operating power level of the laser, in contrast to the optimum transmitting mirror where  $T_{\text{opt}}$ , given by (1.7.3.63), depends on the laser gain.  $K_{\text{opt}}$  depends only on the total losses and saturation parameter. For given losses, the knowledge of  $K_{\text{opt}}$  allows us to define the optimal parameters of the nonlinear crystal, in particular the figure of merit,  $d_{\text{eff}}^2/n_3^2 n_1^2 n_2^2$  and the ratio  $(L/w_o)^2$ , in which the walk-off effect and the damage threshold must also be taken into account.

Some examples: a power of 1.1 W at 0.532  $\mu\text{m}$  was generated in a TEM<sub>00</sub> c.w. SHG intracavity device using a 3.4 mm Ba<sub>2</sub>NaNb<sub>5</sub>O<sub>15</sub> crystal within a 1.064  $\mu\text{m}$  Nd:YAG laser cavity (Geusic *et al.*, 1968). A power of 9.0 W has been generated at 0.532  $\mu\text{m}$  using a more complicated geometry based on an Nd:YAG intracavity-lens folded-arm cavity configuration using KTP (Perkins & Fahlen, 1987). High-average-power SHG has also been demonstrated with output powers greater than 100 W at 0.532  $\mu\text{m}$  in a KTP crystal inside the cavity of a diode side-pumped Nd:YAG laser (LeGarrec *et al.*, 1996).

For type-II phase matching, a rotated quarter waveplate is useful in order to reinstate the initial polarization of the fundamental waves after a round trip through the nonlinear crystal, the retardation plate and the mirror (Perkins & Driscoll, 1987).

If the nonlinear crystal surface on the laser medium side has a 100% reflecting coating at  $2\omega$  and if the other surface is 100% transmitting at  $2\omega$ , it is possible to extract the full SH power in one direction (Smith, 1970). Furthermore, such geometry allows us to avoid losses of the backward SH beam in the laser medium and in other optical components behind.

External-cavity SHG also leads to good results. The resonated wave may be the fundamental or the harmonic one. The corresponding theoretical background is detailed in Ashkin *et al.* (1966). For example, a bow-tie configuration allowed the generation of 6.5 W of TEM<sub>00</sub> c.w. 0.532  $\mu\text{m}$  radiation in a 6 mm LiB<sub>3</sub>O<sub>5</sub> (LBO) crystal; the Nd:YAG laser was an 18 W c.w. laser with an injection-locked single frequency (Yang *et al.*, 1991).

### 1.7.3.3.3. Third harmonic generation (THG)

Fig. 1.7.3.16 shows the three possible ways of achieving THG: a cascading interaction involving two  $\chi^{(2)}$  processes, *i.e.*  $\omega + \omega = 2\omega$  and  $\omega + 2\omega = 3\omega$ , in two crystals or in the same crystal, and direct THG, which involves  $\chi^{(3)}$ , *i.e.*  $\omega + \omega + \omega = 3\omega$ .

#### 1.7.3.3.3.1. SHG ( $\omega + \omega = 2\omega$ ) and SFG ( $\omega + 2\omega = 3\omega$ ) in different crystals

We consider the case of the situation in which the SHG is phase-matched with or without pump depletion and in which the sum-frequency generation (SFG) process ( $\omega + 2\omega = 3\omega$ ), phase-

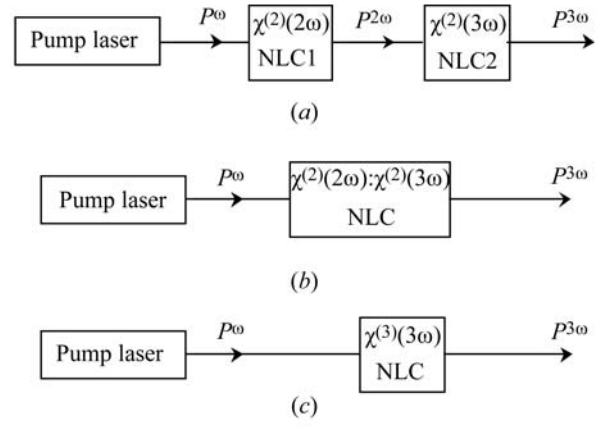


Fig. 1.7.3.16. Configurations for third harmonic generation. (a) Cascading process SHG ( $\omega + \omega = 2\omega$ ): SFG ( $\omega + 2\omega = 3\omega$ ) in two crystals NLC1 and NLC2 and (b) in a single nonlinear crystal NLC; (c) direct process THG ( $\omega + \omega + \omega = 3\omega$ ) in a single nonlinear crystal NLC.

matched or not, is without pump depletion at  $\omega$  and  $2\omega$ . All the waves are assumed to have a flat distribution given by (1.7.3.36) and the walk-off angles are nil, in order to simplify the calculations.

This configuration is the most frequently occurring case because it is unusual to get simultaneous phase matching of the two processes in a single crystal. The integration of equations (1.7.3.22) over  $Z$  for the SFG in the undepleted pump approximation with  $E_1^\omega(Z_{\text{SFG}} = 0) = E_1^\omega(L_{\text{SHG}})$ ,  $E_2^{2\omega}(Z_{\text{SFG}} = 0) = E_2^{2\omega}(L_{\text{SHG}})$  and  $E_3^{3\omega}(Z_{\text{SFG}} = 0) = 0$ , followed by the integration over the cross section leads to

$$P^{3\omega}(L_{\text{SFG}}) = B_{\text{SFG}}[aP^\omega(L_{\text{SHG}})]P^{2\omega}(L_{\text{SHG}}) \frac{L_{\text{SFG}}^2}{w_o^2} \sin^2 c^2 \frac{\Delta k_{\text{SFG}} L_{\text{SFG}}}{2} \quad (\text{W})$$

with

$$B_{\text{SFG}} = \frac{72\pi 2N - 1}{\epsilon_o c} \frac{d_{\text{eff}}^2}{N} \frac{T_3^{3\omega} T_1^\omega T_2^{2\omega}}{\lambda_\omega^2 n_3^3 n_1^\omega n_2^{2\omega}} \quad (\text{W}^{-1})$$

$$a = 1 \text{ for type-I SHG, } a = \frac{1}{2} \text{ for type-II SHG.} \quad (1.7.3.70)$$

$P^\omega(L_{\text{SHG}})$  and  $P^{2\omega}(L_{\text{SHG}})$  are the fundamental and harmonic powers, respectively, at the exit of the first crystal.  $L_{\text{SHG}}$  and  $L_{\text{SFG}}$  are the lengths of the first and the second crystal, respectively.  $\Delta k_{\text{SFG}} = k^{3\omega} - (k^\omega + k^{2\omega})$  is the SFG phase mismatch.  $\lambda_\omega$  is the fundamental wavelength. The units and other parameters are as defined in (1.7.3.42).

For type-II SHG, the fundamental waves are polarized in two orthogonal vibration planes, so only half of the fundamental power can be used for type-I, -II or -III SFG ( $a = 1/2$ ), in contrast to type-I SHG ( $a = 1$ ). In the latter case, and for type-I SFG, it is necessary to set the fundamental and second harmonic polarizations parallel.

The cascading conversion efficiency is calculated according to (1.7.3.61) and (1.7.3.70); the case of type-I SHG gives, for example,

$$\eta_{\text{THG}}(L_{\text{SHG}}, L_{\text{SFG}}) = \frac{P^{3\omega}(L_{\text{SFG}})}{P_{\text{tot}}^\omega(0)} = B_{\text{SFG}}(T^\omega)^4 P_{\text{tot}}^\omega(0) \tanh^2(\Gamma L_{\text{SHG}}) \times \text{sech}^2(\Gamma L_{\text{SHG}}) \frac{L_{\text{SFG}}^2}{w_o^2} \sin^2 c^2 \left( \frac{\Delta k_{\text{SFG}} L_{\text{SFG}}}{2} \right), \quad (1.7.3.71)$$

where  $\Gamma$  is as in (1.7.3.59).